

Report on the representation of vertical velocities in the Iberian Biscay Irish Ocean Analysis and Forecasting system using multi-platform observations



Document type: Master report

Author: Thomas Hermilly

Supervisor: Simón Ruiz

Date: August 2021

Abstract

This report aims at the quantification of the performances of the *Iberian-Biscay-Irish Ocean Analysis and Forecasting system*, a hydrodynamical model based on the quite popular *NEMO Ocean Engine* code. We choose to focus exclusively on the vertical velocity variable, as it has a structure that is still today poorly understood. It is of great interest to understand more accurately the mixing between the top layer and the ocean's interior, and in consequence for nutrient fluxes, phytoplankton bloom and photosynthesis.

The same algorithm retrieving vertical velocities from density arrays thanks to the quasi-geostrophic omega equation is applied to both model data and in-situ measurements corresponding to the same period, to allow comparison. Independent measurements from surface drifters are used to provide another validation method. This data is extracted from the 2018 Calypso cruise dataset, carried out in the Western Mediterranean waters during May and June.

On the sampled front, North-West of the Eastern Alboran gyre, velocities can reach values of 20 m day^{-1} in the upper layer and almost 100 m day^{-1} at a depth of 90 m . The major asset of the model turns out to be a powerful realism of the physical variables, that nonetheless encounters issues in the location and intensity of oceanic phenomena. Amongst other things, we notice an underestimation of velocities of coefficient 4 by the model on the date of the Calypso 2018 experiment.

Contents

1	Introduction	1
2	Context and data	2
2.1	The Alboran sea	2
2.2	The IBI Ocean Analysis and Forecasting System	3
2.3	The Calypso cruise	5
3	Methodology	9
3.1	Processing of model data	9
3.1.1	Data smoothing and resolved scales	9
3.1.2	Dynamic height and geostrophic velocities	9
3.2	Processing of in-situ data	12
3.2.1	Underway CTD sections	13
3.2.2	Surface drifters	14
3.3	The quasi-geostrophic omega equation	15
4	Results	18
4.1	Results from model data	18
4.2	Results from uCTD sections	20
4.3	Results from drifters	21
4.4	Cross-checking with the continuity equation	23
5	Discussion	24
5.1	2D flow and density structure accuracy	25
5.2	Vertical velocities representation	27
6	Conclusion	29
7	List of Figures	30
8	References	31
9	Appendix	34
9.1	Derivation of the quasi-geostrophic omega equation	34
9.2	Vertical velocities numerical integration pseudo-code	36

1 Introduction

Acknowledging the issues of the 21st century, it is of common sense for mankind that it is in the need of predicting its environment more accurately and at larger time scales. Climate change has repeatedly shown its severity over the past decades: observed trends regarding extreme events such as typhoons, cyclones, forest fires, ocean heat waves...etc. tend to reveal themselves quite pessimistic [1]. Even some human populations today are unable to remain where their ancestors were spending their entire lifetime. Although improving this situation nowadays relies more on taking serious measures to avoid those events in particular [2, 3], it relies as well on climate modelling for an enhanced understanding. Increasing our knowledge in this domain is crucial, not only for scientists but also for an entire society suffering from decision-makers ignorance, that serve only economic growth.

Since atmospheric modelling started around 1940, it has known tremendous changes in its resolved spatial and temporal scales. Nevertheless, it cannot be improved today ignoring the key role played by the ocean in weather prediction [4]. Indeed, the inconceivable heat capacity of the ocean makes it one of the main factors constraining the atmospheric state and it has justifiably reached a state-of-the-art level of interest for modellers today. On top of that, predicting the ocean state is needed in particular to predict events happening directly in the ocean: acting for the preservation of marine ecosystems is of serious anthropogenic interest today [5] and it could be enhanced by forecasting heatwaves, preventing fishing in sensitive areas...etc.

Furthermore, the vertical velocities variable is of a very serious importance regarding ocean-atmosphere exchanges: it is a quite direct quantity to understand the mixing of the surface layer with the interior of the ocean, which is almost totally cut off from the atmospheric oxygen, light and winds. Phytoplankton for example, which is responsible for a carbon recycling of about 50 gigatons each year [6], needs both nutrients and light to subsist. This means that nutrient fluxes — that are mostly vertical due to nutrients location [7] — crossing the euphotic layer¹ are places where phytoplankton is more likely to bloom, and in consequence recycle inorganic carbon [8]. Due to the 3 to 4 orders of magnitude difference separating vertical velocities from horizontal currents in intensity, their measurement remains today a real challenge.

¹This layer corresponds to the layer receiving energy from sunlight.

In order to build more consistent models, modellers need validation from people that use their algorithms, so that the effort is first put into what is of interest for users. Hence, this report aims at qualifying the assets and drawbacks in terms of vertical velocities of the *Iberian Biscay Irish Ocean Analysis and Forecasting System* [9], which provides a 5-days forecast of hydrodynamical variables in the North-Western Atlantic including the western Mediterranean. In section 2, the data used to carry out this work will be described. Section 3 details the computations carried out in order to retrieve the vertical velocity variable. In section 4, associated results will be presented. The discussion related to these results is developed in section 5, and finally conclusions are drawn in section 6.

2 Context and data

2.1 The Alboran sea

Relatively to the five oceans, the Mediterranean can be considered a small-sized experiment basin for Oceanography. The large-scale phenomena observed in the outer ocean are all detected at smaller scales in the Mediterranean, thus allowing an easier leading of Oceanographic campaigns and in-situ measurements. Indeed, even though this basin is smaller than the open ocean, we can see on figure 1 that the Rossby radius¹ in this region is low because of the relatively shallow water depth. In other words, it allows the rotational effects to appear at smaller scales.

The Alboran Sea is the westernmost region of the Mediterranean, spreading on about 400 km from Gibraltar to Almeria and Oran. It corresponds to the location where Atlantic waters enter the Gibraltar strait and meet Mediterranean waters (figure 2). Knowing the Southern European climate and closed-basin shaped sea shore occurring there, it is understandable that heat and evaporation make the water masses very salty compared to the mixed Atlantic waters. The Alboran sea is thus an adequate place to observe a mesoscale² mixing between two water masses with very different properties (figure 3). This document focuses specifically on this very active area.

¹Defined as $\sqrt{\frac{gH}{f}}$ with g the gravitational acceleration, H the water depth and f the Coriolis frequency, it represents an order of magnitude from which planetary effects become significant regarding phenomenon such as gravity waves or buoyancy.

²Scale ranging spatially from 10 km to 100 km. In the ocean, it corresponds to times scales ranging from 2 to 20 days.

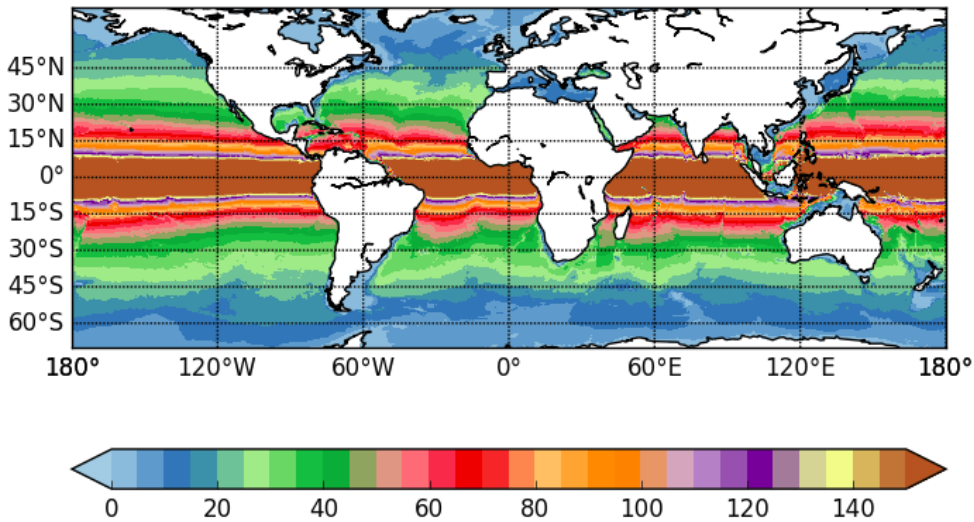


Figure 1: World map of the Rossby radius (km) [10].

The main phenomena resulting from these particular conditions are an oceanic density front and two quasi-permanent mesoscale gyres aligned zonally [11] (figure 2). In the literature, they are respectively referred to as Almeria/Oran front, Western and Eastern Alboran gyres. Besides, we observe in this location secondary yet serious phenomena such as filaments, meanders, internal waves...etc. Notably, as a great part of the flow occurs along isopycnals [12] which in this case are relatively steep, the permanent fronts are hosting significant values for vertical velocities and in consequence important chlorophyll quantities from phytoplankton bloom, as shows figure 4.

2.2 The IBI Ocean Analysis and Forecasting System

The model used here is the *Iberian Biscay Irish Ocean Analysis and Forecasting System* (IBI model), which is one of the operational models of the *Copernicus Marine Environment Monitoring Services*¹. It consists in a NEMO² 5-days hydrodynamic forecast of several variables. This work uses a daily average of its output. Besides the prediction equations [14] not detailed in this report, the model applies a daily assimilation of in-situ temperature and salinity profiles, Sea Surface Temperature (SST) and Sea Surface Height (SSH) from satellite imagery. The variables used for this work were potential temperature and salinity (figure 5), zonal and meridional total water flow components. The horizontal

¹Marine branch of the European Copernicus Programme. It is a free service supporting ocean research that provides a wide range of datasets [13].

²Nucleus for European Modelling of the Ocean is an ocean modelling structure developed by the NEMO System Team of the Pierre-Simon Laplace Institute in Guyancourt.

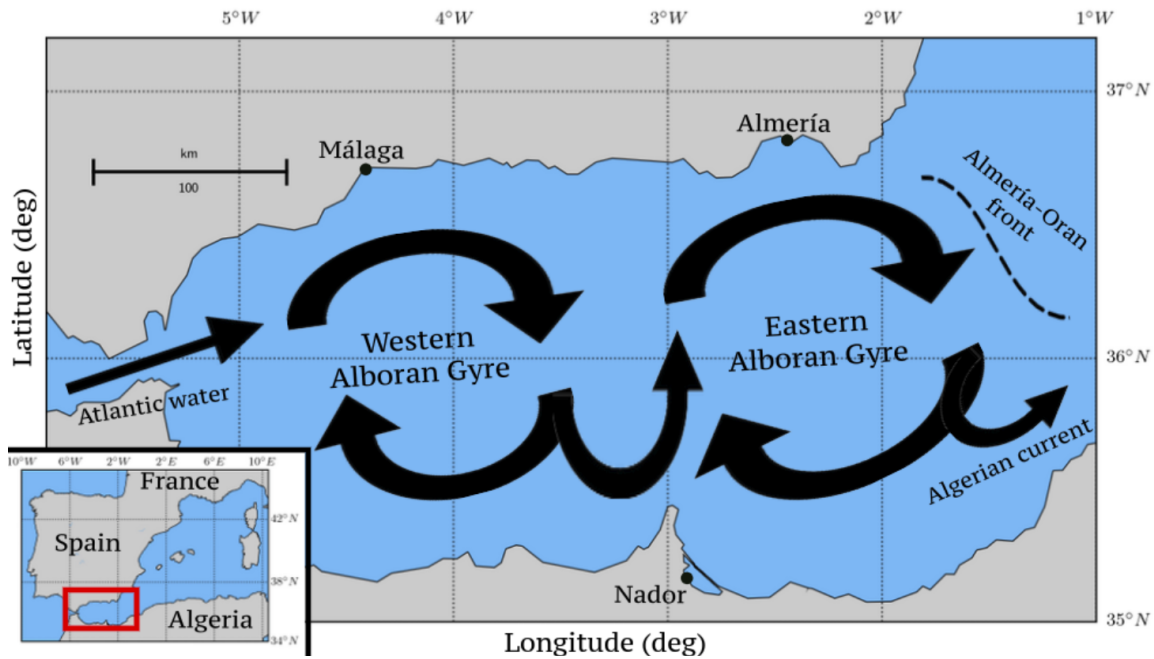


Figure 2: The Alboran sea surface circulation.

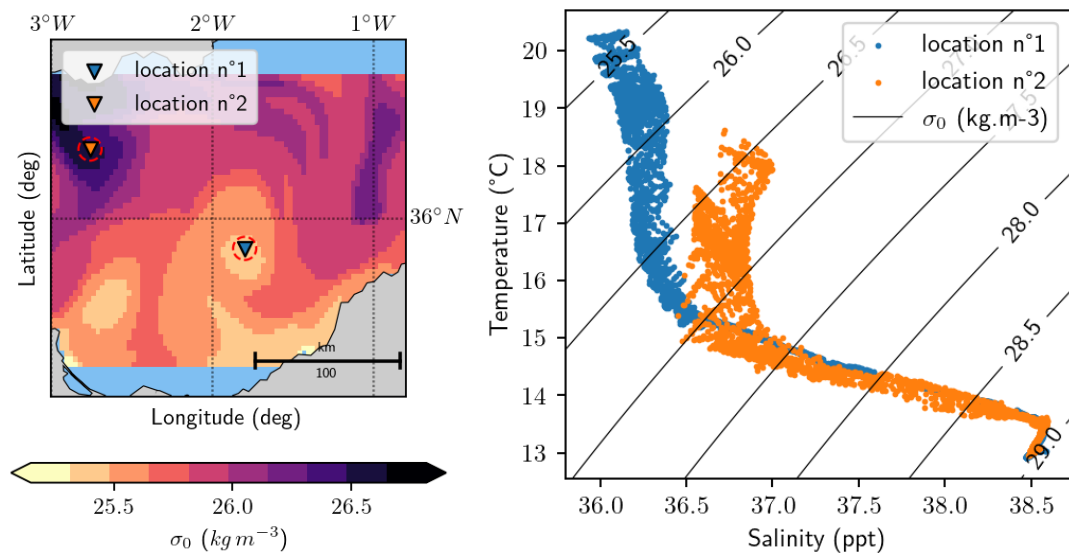


Figure 3: IBI model temperature and salinity profiles on June 1st, 2018.

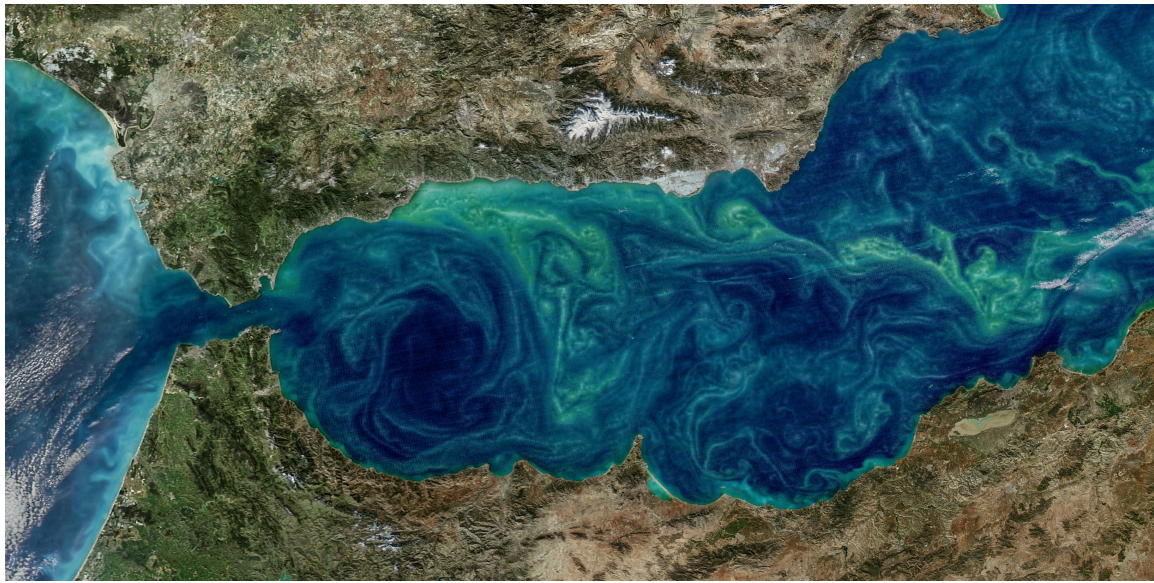


Figure 4: Satellite image of chlorophyll in the Alboran sea on January 17th, 2018 (NASA).

grid resolution is approximately of 2.5 km in longitude and 3 km in latitude, which leads to deriving variables resolving well the mesoscale, up to the submesoscale¹. The vertical levels are not regular since a higher resolution is needed in the top layer as a consequence of the important density gradients resulting from air-water exchanges, whereas deep in the ocean's interior, one does not need a lot of vertical resolution to reflect a certain homogeneity. Therefore, the vertical grid spacing goes from about 1 m at surface down to 500 m at 5000 m depth. It takes as well into account various processes such as tidal forcing, surges, fresh-water discharges from rivers...etc. that strongly influence the output variables [9].

2.3 The Calypso cruise

The in-situ measurements associated to this research has been acquired in the frame of the Calypso experiment. This campaign has been led between 2017 and 2019 on various ships, and aims at the detection of 3D features that play a role in the mixing of the seawater top layer with the ocean's interior, at the sub-mesoscale up to the kilometric scale. In 2018, the Italian NATO vessel *NRV Alliance* [15] collected the data in the area of a semi-permanent front at the West of the Eastern Alboran gyre, few tens of kilometres South of Almeria. To survey this area, the ship was equipped with a quite innovative set

¹Scale ranging spatially from 1 km to 10 km . Associated time scales are respectively hours to 1-2 days.

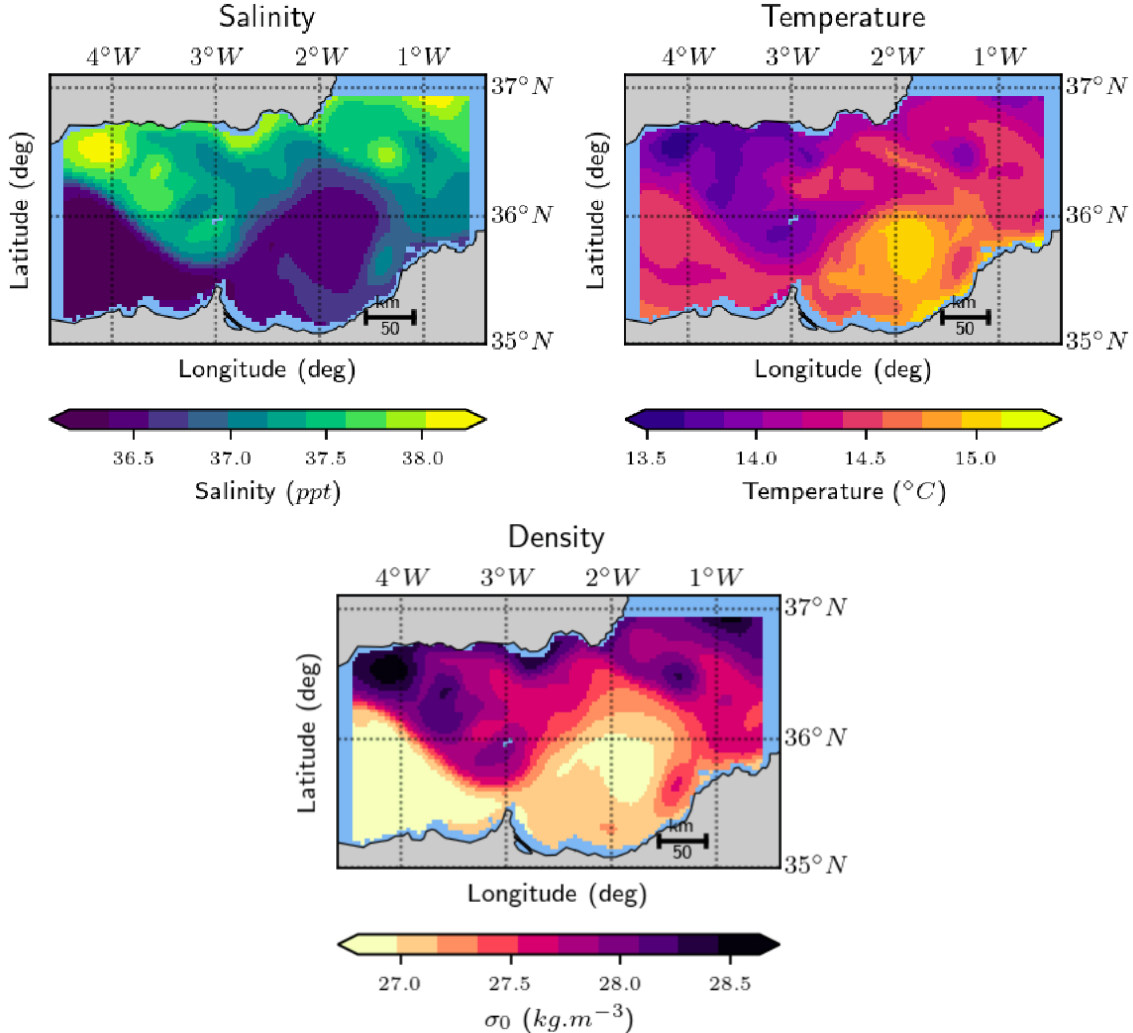


Figure 5: Salinity and potential temperature on April 7th, 2018 at 60 m depth from the IBI model, and resulting density using the thermodynamic equation of sea water.

of sensors shown figure 6:

- Various surface drifters: CARTHE [16, 17], CODE [18, 19] and Surface Velocity Program (SVP) [20]
- Lagrangian float [21] equipped with Acoustic Doppler Current Profiler (ADCP)
- Hull-mounted ADCP and thermosalinograph
- Conductivity Temperature Depth (CTD) rosette, underway CTD [22, 23] and eco CTD [23]

The surface drifters were all meant to measure the 2D velocity field. Some SVP drifters measured the 15 m deep horizontal current thanks to a drogue centred on that

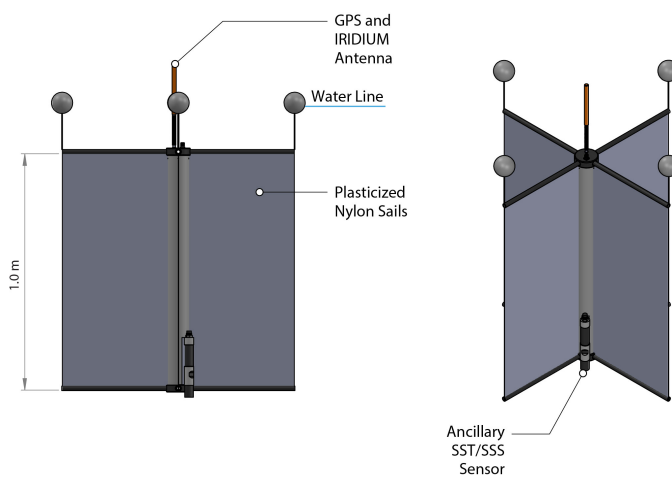
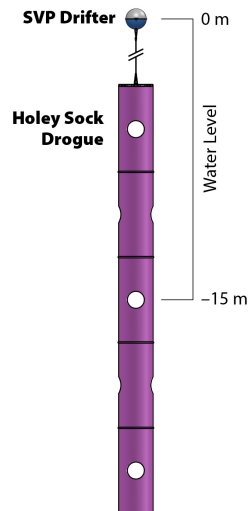
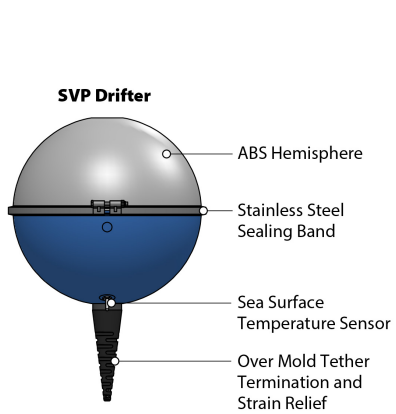


Figure 6: From left to right and from top to bottom: the Alliance ship [15], CARTHE drifters [17, 16] (picture: S. Ruiz (IMEDEA-CSIC)), the Lagrangian float drifter equipped with ADCP (picture: S. Ruiz (IMEDEA-CSIC)), a SVP drifter [20], a CODE drifter [19] and an uCTD probe [22].

level [24]. The Lagrangian float maintains a density close to its surroundings in order to measure directly the vertical component of the flow. In addition, an ADCP sensor heading up was mounted on it to measure the vertical velocity component subtracting the drifter's depth gradient. The ADCP and thermosalinograph mounted on the ship's hull were mainly used to estimate the location of the front while sailing. Finally, CTD profiles with the rosette were done regularly on the track, and underway CTD (uCTD) and eco CTD probes were continuously towed up and down to have salinity, temperature and chlorophyll vertical sections (figure 7) [23].

From all the measurements done during this experiment, there are ways to retrieve the vertical component of the water flow: the Lagrangian float measures the variable of interest both directly through its own motion and indirectly with the ADCP sensor. From the different CTD sections, it is possible to construct 3D arrays of salinity and temperature using optimal interpolation, kriging or even multivariate analysis [25]. After that, the processing line consists essentially in computing successively density, dynamic height, geostrophic currents and finally use the simplified Navier-Stokes equations to deduce the vertical motions (*e.g.* using the quasi-geostrophic Omega equation). This methodology is fully detailed in section 3. At last, it is possible to use the data coming from the surface and 15m buoy drifters to derive the divergence of the horizontal velocity fields on these two levels. Integrating this data according to the simplified continuity equation under a synoptic assumption gives an estimate of the vertical velocities in the upper layer [24].

Both the uCTD sections and the surface drifter data from this cruise are exploited as a reference to compare with the model output, in the following sections.

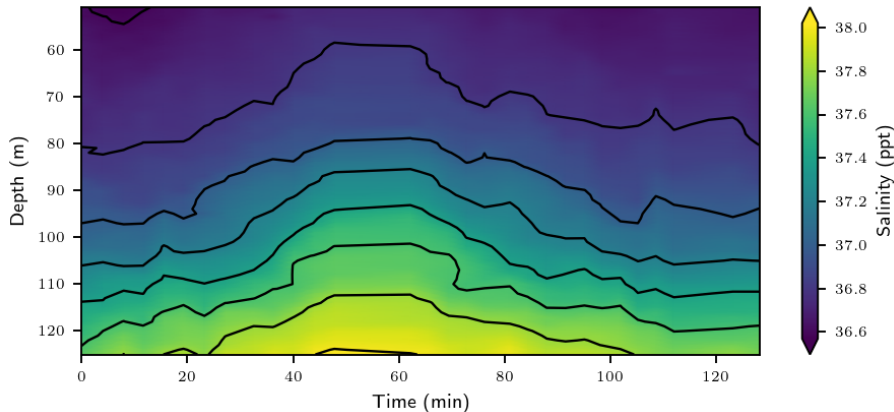


Figure 7: Calypso 2018 dataset: salinity vertical section from uCTD crossing the front both ways.

3 Methodology

3.1 Processing of model data

As a first step, we present the methodology to derive the useful variables that will result in vertical velocities.

3.1.1 Data smoothing and resolved scales

The IBI model resolution is about 3 km horizontally. Therefore, we have to avoid the resolution of scales smaller than 6 km according to the Shannon-Nyquist criterion¹, that represents a theoretical minimum to respect. However, we can choose to apply a bigger smoothing radius in order to also erase scales that are not well resolved by the sampling, because they can be responsible for the propagation of errors when successive derivatives are computed. In order to get a clear scale-smoothing value R as a parameter, we use a radial-based bicubic filter which uses a maximum search radius, and smoothes the centre point thanks to a R -scaled bicubic weighted average:

$$r \longrightarrow \begin{cases} (1 - (\frac{r}{R})^3)^3 & \text{if } r < R \\ 0 & \text{else.} \end{cases}$$

Figure 8 shows that after applying this filter with a R -value of 7 km , the main features remain on the images. Secondly, the difference between the original output and the filtered temperature and salinity displays erased features of about the smoothing radius. We observe an alternation of positive and negative lines in the difference, confirming that the filter actually fulfilled the data smoothing. The maximum thickness of the difference patterns (considering the size of one positive and one negative area) is at maximum of 6 grid spacings. As the Shannon-Nyquist criterion tells to filter at least twice the size of the grid spacing, this filtering takes out features that are three times bigger. This will allow us further to focus on general patterns, of a size bigger than 10 km , and at the same time give us more certitude about the further observed patterns, that will not attempt to show unresolvable features.

3.1.2 Dynamic height and geostrophic velocities

With the smoothed salinity and temperature as 3D arrays, we can now carry out further steps to achieve the vertical velocities computation.

¹This criterion states that in order to resolve a particular scale, the spatial sampling frequency must be superior to half of the scale in question.

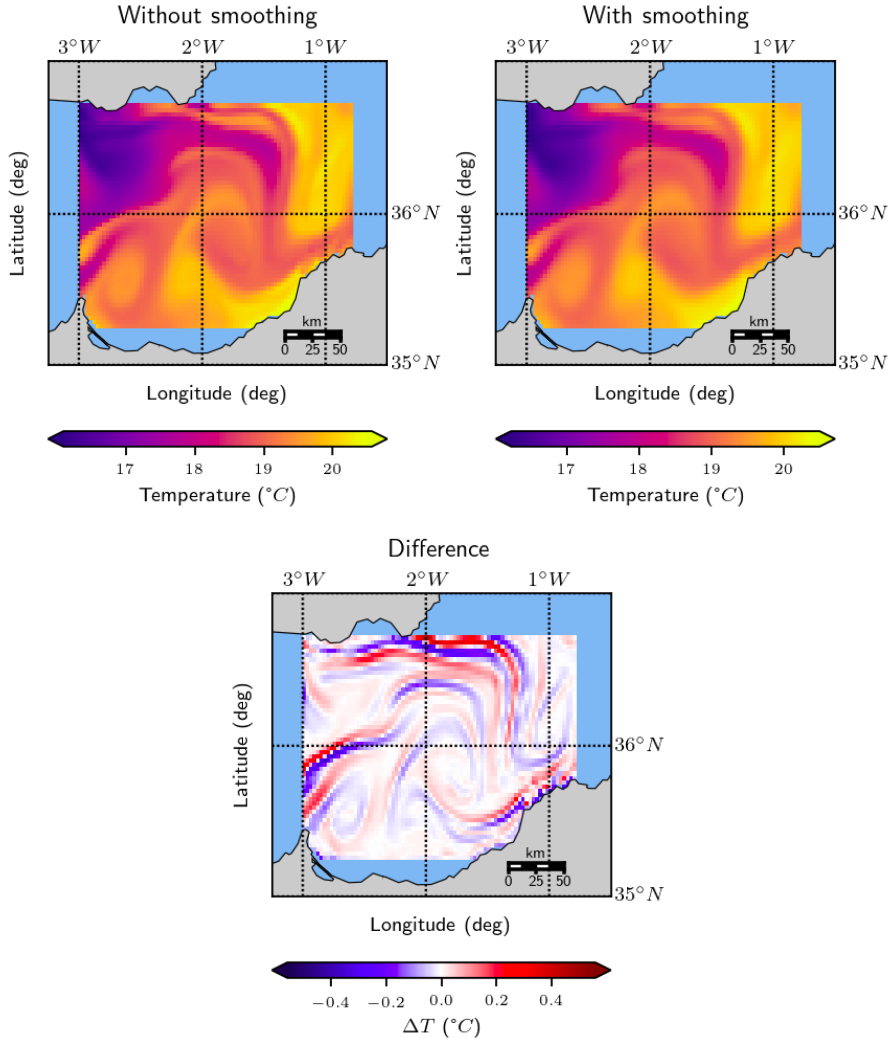


Figure 8: Model potential temperature on June 1st, 2018 without and with 7 km radius bicubic smoothing and resulting difference.

Together with the Boussinesq approximation¹, conservative temperature and salinity is enough to derive the potential density variable thanks to the thermodynamic equation of seawater. Indeed, the relation between pressure and depths allows the derivation of conservative temperature from potential temperature, and the work of *Millero and Poisson, 1981* [26] gives a polynomial equation of seawater in conservative temperature and salinity deduced from measurements.

¹This approximation considers the horizontal density gradients negligible facing its vertical gradients.

Yet, the density gives us information about the volume of a square-metre of seawater and in fact, the inverse of density defines the specific volume, which can be numerically integrated from a no motion level up until a depth z to give dynamic height [27]. This quantity relates of a height anomaly at each vertical level in the fluid and can be used as a streamfunction for geostrophic flow under the Boussinesq approximation [28]: $\frac{\partial p(x,y,z)}{\partial x} \approx \rho_0 g \frac{\partial z(x,y,z)}{\partial x}$. In other words, the geostrophic flow is fully defined by dynamic height using the geostrophic balance:

$$\begin{cases} f_0 u(x, y, z) = -\frac{1}{\rho_0} \frac{\partial p(x, y, z)}{\partial y} \implies u(x, y, z) = -\frac{g}{f_0} \frac{\partial H(x, y, z)}{\partial y} \\ f_0 v(x, y, z) = \frac{1}{\rho_0} \frac{\partial p(x, y, z)}{\partial x} \implies v(x, y, z) = \frac{g}{f_0} \frac{\partial H(x, y, z)}{\partial x} \end{cases}$$

with f_0 the Coriolis coefficient, ρ_0 the mean density, g the gravity acceleration, u and v respectively the geostrophic zonal and meridional water flow components, p the local pressure and H the dynamic height. In fact, the geostrophic flow lines follow the dynamic height isolines, and has a module proportional to its gradient.

The previously mentioned no-motion level has to be chosen carefully though. We are looking for a water depth at which the fluid is at rest, to be able to integrate dynamic height from here. This value depends a lot on the location in question, and for the Alboran sea can usually be chosen from 200 m downward [29].

In fact, knowing that most of the water flow is occurring along-isopycnals¹ [12], the reference level should be chosen a little bit deeper than 200 m in order to consider the whole eddy signature: as figure 9 demonstrates, the eddy potential density signal goes down to about 250 m on June 1st, 2018. Nonetheless, it has to be chosen shallow enough in order both to remain not excessively computationally costly with smaller 3D arrays, and to avoid including too many bathymetry sections in the domain as it causes more uncertainty relatively to dynamic height and creates unwanted edge effects.

To be more specific, when bathymetry exceeds the no-motion level, the integration must be performed filling the bathymetry holes with the nearest neighbours in latitude or longitude in the density arrays [30]. For instance, if one chooses to fill with the nearest latitude neighbours, the output will have no meridional gradient in dynamic height, and in consequence have no zonal geostrophic velocity at this level. Even after applying the bathymetry mask to the dynamic height array, we have to keep in mind that the arrays may contain synthetic values just above bathymetry, that are only meant to estimate the

¹Surfaces of constant density.

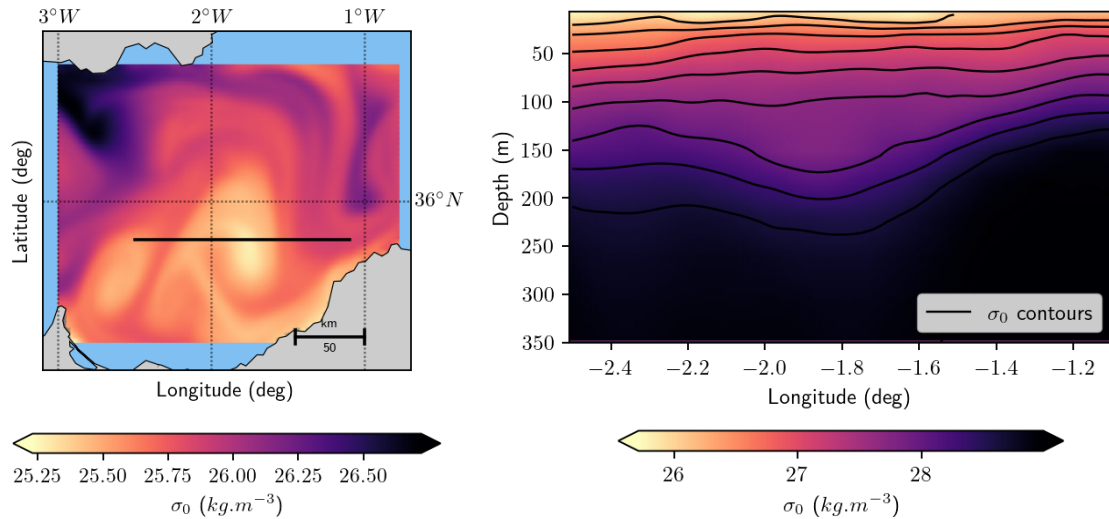


Figure 9: IBI model surface values with transect location and vertical section of potential density referenced to surface level on June 1st, 2018.

upper layers values after integration.

With the derivation of these new variables — density, specific volume, dynamic height and geostrophic velocities —, we can proceed to the estimation of the vertical component of the flow using the quasi-geostrophic omega equation (further details about this approximation are given later, in section 3.3 and in [Appendix 9.1](#)).

3.2 Processing of in-situ data

As assessed in section 2.3, there is a way to estimate vertical velocities from all the sensors used in the 2018 Calypso experiment (various CTD sections, Lagrangian float and surface drifters). However, there may be a problem in the comparison with the variable derived from the model output in terms of resolved scales. For instance, the lagrangian float data consists only of short and shallow high resolution dives (less than 2 km long and less than 10 m deep) that make its data impossible to compare to the model output, as it resolves the sub-kilometric scale. This section is therefore dedicated to detailing the method to retrieve vertical velocities from the in-situ measurements of the 2018 Calypso cruise using uCTD sections and surface drifters, which both characterize scales that the IBI model can resolve.

3.2.1 Underway CTD sections

The dataset exploited in this section is a non-regular sampling of a $15 \times 60 \text{ km}$ area, located 2.25°W and 36.25°N . On the day of the survey, the 1st of June 2018, at this location, a strong North-South front had been detected as shown by the altimetry record on figure 10: it corresponds to the separation of Atlantic and Mediterranean waters North-West of the Eastern Alboran gyre.

As the dataset consists of only two variables (potential temperature and salinity), and as well regarding the small size of the domain relatively to the scales of interest, multivariate analysis interpolation in this zone is unnecessary, even if it has been shown to reach better performances than univariate optimal interpolation [31]. To compensate for the sampling irregularities, we chose here to compute potential density from temperature and salinity, and to use an ordinary kriging¹ method because this operator handles sparse measurement properly: it takes into account the distance between observations and gives more importance to spots that are isolated spatially. Conversely, areas with a lot of observations will be granted a decreased weight in the final interpolation to compensate for measurements redundancy. As we want to keep the vertical stratification intact, 2D-kriging has been performed at every level (figure 10 bottom left) using a specific spherical variogram² interpolated on the experimental variogram. In fact, as density varies quickly along the z -axis, 3D kriging would create influence from upper and lower layers on values in the current layer, which we do not want. The range parameter turned out to be about 4 km .

Finally, the bottom right panel of figure 10 shows an envelope of variance around the observation sites which indicates the level of confidence we can have in the interpolation value at a certain location. When looking away from the observation sites, we must keep in mind that the values get more and more synthetic, and hence the edges of our domain are to be considered more uncertain.

With the uCTD data exploited at this point, let us now focus on the surface drifters data that require a very different processing.

¹This interpolation operator is the best linear unbiased estimator in the sense that it minimizes the variance of the output field.

²Function giving spatial dependence from distance between points for a specific variable.

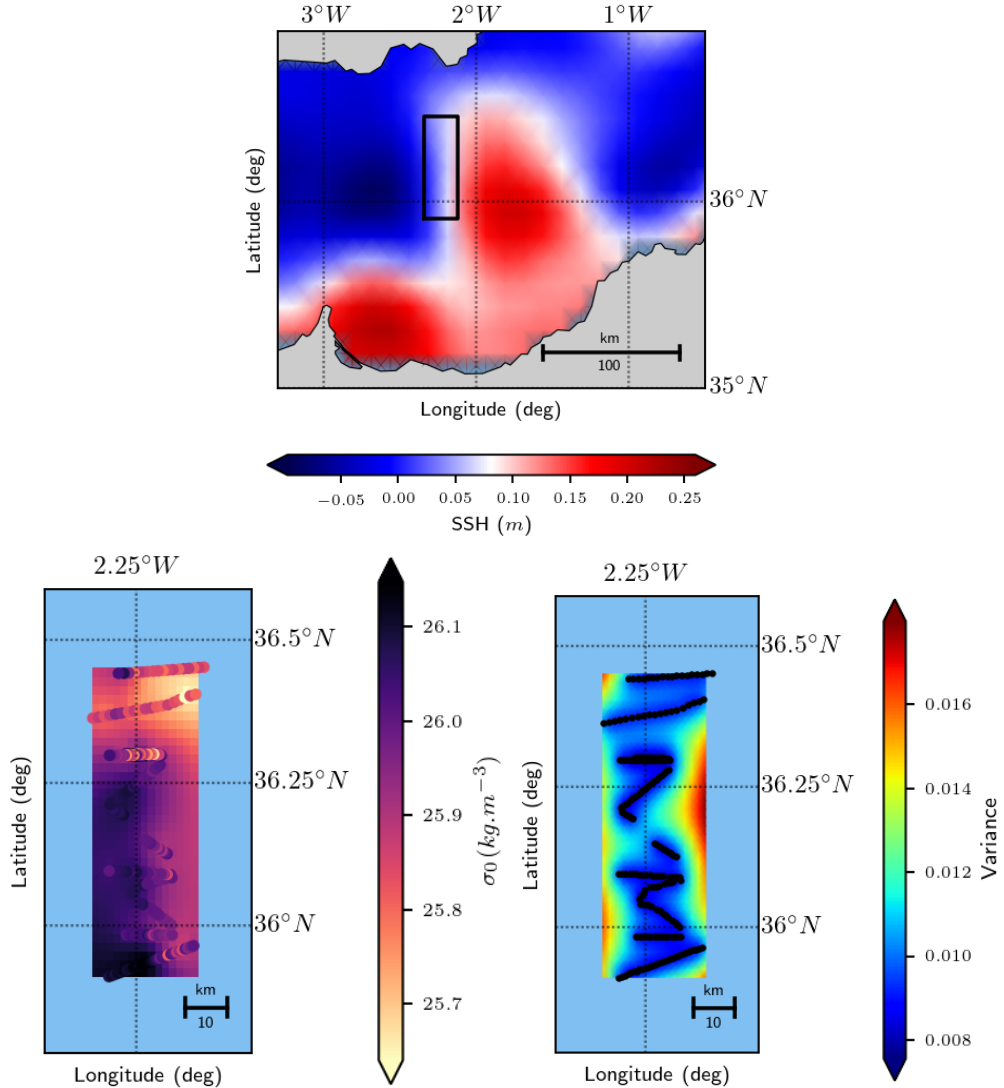


Figure 10: Sea Surface Height from satellite altimetry on June 1st, 2018 (top), surface CTD transects values and kriging interpolation (bottom left), surface CTD transects location and kriging variance (bottom right).

3.2.2 Surface drifters

In this section, the data in question is the 2D velocity fields from drifters at surface and at 15 m depth. The data used here is the work of *Tarry et al., 2021* [24], which gives more details about it.

From triplets of drifters or more, it is possible to determine whether the field is diverging or converging adjusting its gradients using least-squares in the following

Taylor expansion:

$$u_i \approx \bar{u} + \frac{\partial u}{\partial x}(x_i - \bar{x}) + \frac{\partial u}{\partial y}(y_i - \bar{y})$$

\bar{u} being the polygon barycentre zonal speed, \bar{x} and \bar{y} its position coordinates in the horizontal plane, u_i the drifter speed and x_i and y_i its position coordinates in the horizontal plane. The same equation applies for the meridional speed. Using all possible combinations¹ of more than 80 drifters leads to an homogeneous estimated field included in the drifting area. Integrating from surface to 15 m the opposite of the horizontal divergence field gives an estimation of vertical velocities according to the continuity equation:

$$\frac{\partial u}{\partial x} + \frac{\partial v}{\partial y} + \frac{\partial w}{\partial z} = 0$$

noting the along x , y and z water flow components respectively u , v and w . With this assumption and a null boundary condition at surface, we can write:

$$w(D) = \int_{z=0}^D \left[\frac{\partial u}{\partial x}(z) + \frac{\partial v}{\partial y}(z) \right] dz$$

keeping in mind that the z -axis is oriented down.

The code of Tarry *et al.*, 2021 [24] has been run to obtain the divergence field and then an estimation of vertical velocities. Contrary to the CTD sections, this method characterizes the sub-mesoscale and is impossible to be considered synoptic. Temporal variations of the field are visible when adjusting the gradients to new polygons and speeds at every time discretization. Nevertheless, it can help us in the quantification of model errors through the understanding of the value-span of vertical velocities in the upper layer.

3.3 The quasi-geostrophic omega equation

Instead of using the continuity equation to derive an estimation of the vertical component of the flow, we can avoid assuming the complete incompressibility of water parcels using the quasi-geostrophic omega equation. It is derived from the equations of motion using the Boussinesq, quasi-geostrophic velocities and mesoscale assumptions (a detailed derivation is provided in **Appendix 9.1**). It can be written as follows [32]:

¹We must erase some clusters: polygons that are too big or too small regarding the scales we want to resolve, quasi-aligned clusters...etc.

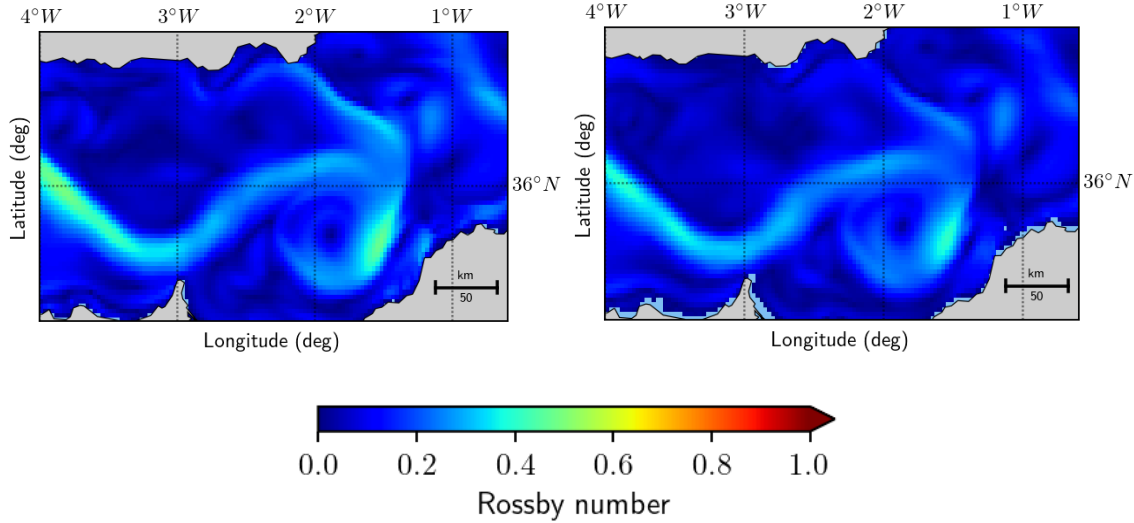


Figure 11: Rossby number associated to model currents on April 7th, 2018 at surface (left) and at 150 m (right). Characteristic scale of 30 km.

$$N^2 \left(\frac{\partial^2}{\partial x^2} + \frac{\partial^2}{\partial y^2} \right) w + f_0^2 \frac{\partial^2 w}{\partial z^2} = 2 \vec{\nabla} \cdot \vec{Q}$$

with N the Brunt-Vassala frequency, f_0 the Coriolis frequency, and

$$\vec{Q} = \frac{g}{\rho_0} \left(\frac{\partial \vec{u}_g}{\partial x} \cdot \vec{\nabla} \rho'; \frac{\partial \vec{v}_g}{\partial y} \cdot \vec{\nabla} \rho' \right)$$

a vector representing a forcing term.

Figure 11 shows that in the Alboran sea, the required quasi-geostrophic assumption is sometimes compromised. Areas where the Rossby number¹ associated to the flow is bigger than 0.4 are not rare when the water flow exceeds a speed of 0.7 ms^{-1} . Therefore, we take note that the quasi-geostrophic hypothesis may reach its limits at some point, later in this study.

As the quasi-geostrophic omega equation does not allow analytical solutions, we choose an iterative finite differences algorithm to solve it using our variables (a pseudo-code of this algorithm is given in the **Appendix 9.2**). It consists of applying successively the following quasi-geostrophic omega equation as finite differences to the current array,

¹Dimensionless value indicating whether rotational effects will be negligible with regards to a specific fluid flow. It can be defined as $R = \frac{u}{f L_c}$ with u the intensity of the fluid velocity, f the Coriolis acceleration and L_c the characteristic spatial scale of interest.

starting from a null array and until convergence:

$$w_{i,j,k} = -\frac{1}{2}\left(\left(\frac{N_k}{\Delta x}\right)^2 + \left(\frac{N_k}{\Delta y}\right)^2 + \left(\frac{f_0}{\Delta z_k}\right)^2\right)^{-1}\left(F_{i,j,k} - N_k^2 \frac{w_{i-1,j,k} + w_{i+1,j,k}}{\Delta x^2} - N_k^2 \frac{w_{i,j-1,k} + w_{i,j+1,k}}{\Delta y^2} - f_0^2 \frac{w_{i,j,k-1} + w_{i,j,k+1}}{\Delta z_k^2}\right)$$

noting i , j and k the indexes for resp. the x , y and z axis, their grid spacings Δx , Δy and Δz and $F = 2\vec{\nabla} \cdot \vec{Q}$ the forcing term. Written like this, the integration considers an irregular vertical grid spacing to be more general, but in our case the vertical profiles of the Brunt-Vassala frequency and the forcing term have been interpolated on a 10 m spaced discretization of the axis using piecewise cubic splines, in order to match the work of *Pascual et al. 2004* [33] that have obtained coherent results with this value.

In fact, it can easily be shown that the output values are sensitive to the grid spacing on the z -axis, and thus it has to be thought out with consideration. One can understand this sensitivity via developing the product in the previous finite differences equation: the first three terms all turn out to go towards 0 when Δz_k goes to 0, but the last term is proportional to:

$$\frac{w_{i,j,k-1} + w_{i,j,k+1}}{1 + \left(\frac{N_k \Delta z_k}{f_0 \Delta x}\right)^2}$$

which goes to $w_{i,j,k-1} + w_{i,j,k+1}$ when $\Delta z_k \rightarrow 0$ instead. In other words, by transitivity, it is equivalent to the setting of an infinite weight to the first and last layers of vertical velocities values in the calculation of w at a particular level, and thus makes the interior of the velocities array tending towards boundary conditions, which are null in our case. After several tries over grid spacings, a constant Δz value higher than 7m is recommended in order for the boundary conditions not to overspread. Of course, an excessively high value will make the z -axis poorly sampled, and should be avoided as well.

In our case, the boundary condition has been set to zero on top, bottom and edges. Indeed, there cannot possibly be any vertical motion in average at surface, and at the bottom of our domain we choose to assume no motion. On the edge though, the condition has been set to zero even if velocities are not assumed to be null, because of the horizontal spatial convergence which is quite quick: about 2 grid nodes are required

to observe spatial convergence (not shown). Regarding the grid spacing, this represents about 5 km which is usually very small compared to the size of the computation domain. In other words, the estimation of vertical velocities on the edges for a correct boundary condition remain almost impossible at the moment, and in any case the interior of the velocities array is not sensitive to the edge values with this method.

Furthermore, the threshold terminating the iterative algorithm has been chosen to fulfil a full convergence using the decreasing rate between previous velocities and their update. The algorithm was thus stopping at a rate corresponding to a maximum change of 0.1% after a thousand iterations (observations shows that this integration has strictly decreasing residuals). In most cases, about 200 loops and 70 minutes were needed to reach such convergence with a $29 \times 54 \times 72$ grid.

Apart from the surface drifter dataset, the results presented in section 4 have been derived with this method.

4 Results

In general, it is noticeable that the quasi-geostrophic omega equation integration draws successive patterns changing sign with the gradient of the dynamic height isolines radius and increasing with its gradient (figure 12). In consequence, the most active zones in our case in terms of vertical velocities are the edges of the two gyres, which are strong fronts. In places where the dynamic height gradient is of 0.3 m for 100 km , involved speeds are of about 30 m day^{-1} at 60 m .

4.1 Results from model data

For the model output, runs have been performed in different areas of the Alboran sea at various dates. The no motion level has been set to 300 m , and experience shows that up to 150 m , the output is not significantly influenced by this choice neither in intensity nor location of maximum speeds (not shown). However, edge effects play an emphasized role when reducing the size of the domain. The smoothing radius of the raw variables (figure 5) has been set to 5 km , which prevents the popping of too many smaller features on the vertical velocities maps. Nevertheless, gradients calculations near bathymetry results in small features appearing. These unwanted edge effect have to be taken out of scope by the reader (35.5°N , 2°W on figure 12 maps).

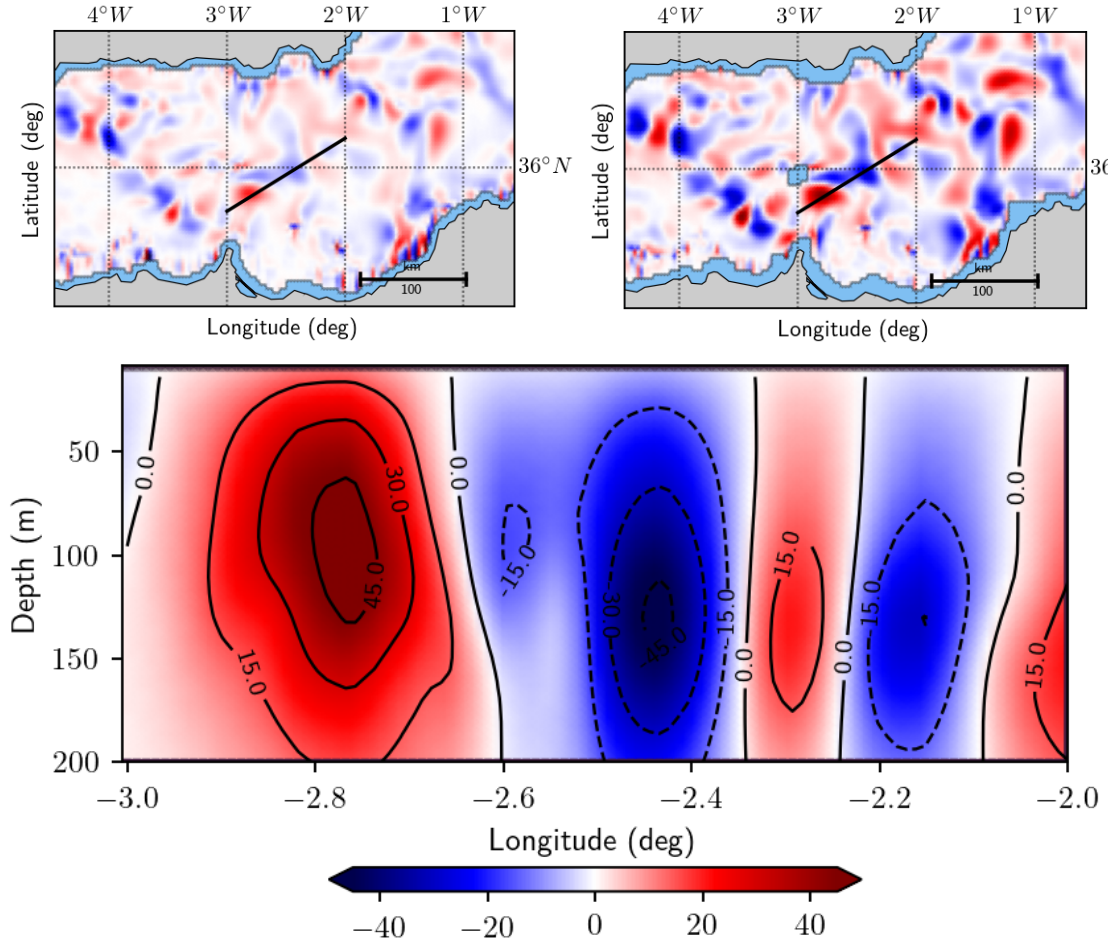


Figure 12: Vertical velocities from IBI model variables on April 7th, 2018 at 20 m (top left) and 60 m (top right) with section location (black line) and associated vertical section (bottom).

Like it has been assessed in the previous section, the vertical velocities from the quasi-geostrophic omega equation are located on the sides of the eddies in places where the geostrophic currents are intense. This leaves the interior a relatively passive area, where velocities are an order of magnitude below. Maximum values are usually located between 50 m and 100 m and are up to 50 m day^{-1} in our zone. This occurs during spring and autumn transition periods, when the Alboran sea is more active [29] (figure 12).

4.2 Results from uCTD sections

In the case of this data, the no motion level has been set higher at 150 m , as only few data has been retrieved at lower levels. Using only the few measurements carried out below this layer, the kriging algorithm would perform a considerably synthetic interpolation which we are willing to avoid. The major drawback of the uCTD data is that it leads to losing a lot of spatial resolution as a result of the transects spacing, whereas along-track resolution is very high. Hence, the smoothing search radius has been set to 5 km — reaching then a diameter of 10 km — as the sections were approximately 5 km spaced. Attempting the resolution of smaller scales turns out to be impossible regarding the spatial distribution of the measurements. It is important to keep in mind that as the transects are not parallel, their spacing changes along track. It makes the minimum scale resolution parameter of the filter complicated to choose. Therefore, this choice of a 5 km radius has been done checking the vertical velocities resulting from the kriging, for which this particular value seems to be enough to efficiently erase features smaller than 5 km . On top of that, the kriging parameters perform through the adjusted variograms another operation of smoothing parametrized with actual statistical information about local density and in this way prevents from the start such problem to appear.

Furthermore, we assume here that the scalar field is synoptic, whereas about 10 hours have been spent at sea to retrieve the uCTD data in the night between the 31^{st} of May and the 1^{st} of June. At this daily time scale, the front moved and therefore, our vision of it through the uCTD sections is slightly distorted. However, this hypothesis remains valid for the analysis of the mesoscale signal of the front, since this time (10 hours) is much smaller than the usual time window (2-3 days) assumed in this study [34, 35].

On figure 13, one can see that like the model data, the uCTD data displays successive patterns with an alternation of sign along the front. The variations of the dynamic height radius are stronger in the North of the area and so imply higher values for the vertical component of the flow at a latitude of 36.3°N . The highest value is about 70 m day^{-1} and the lowest of about -100 m day^{-1} , both located approximately 90 m deep. The main features appearing have an horizontal size of about 10 km .

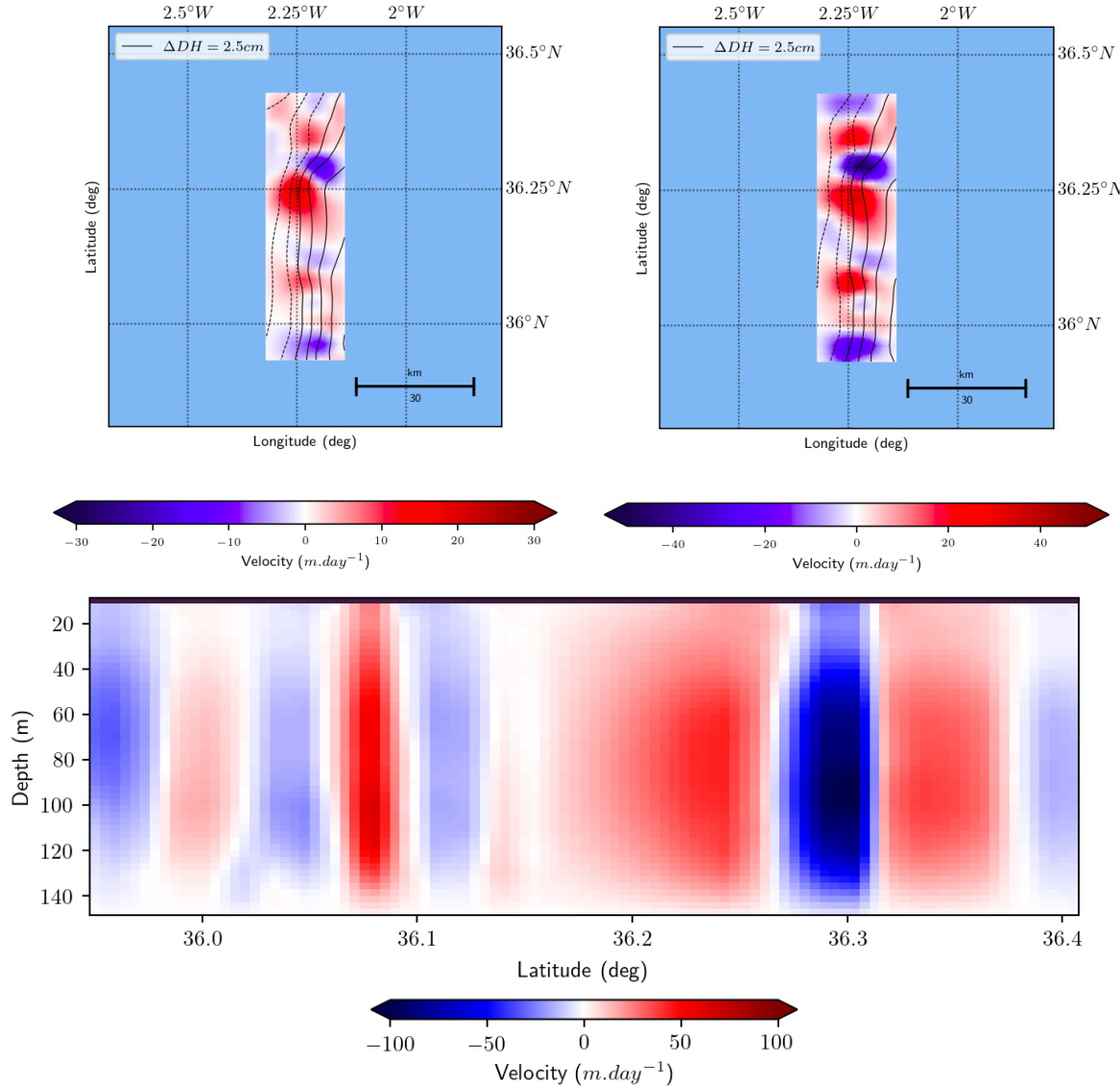


Figure 13: Vertical velocities from uCTD variables on 1st June, 2018 at 20m, 60m depths with dynamic height isolines and its associated vertical section along latitude (at 2.25°N fixed longitude).

4.3 Results from drifters

The 82 drifters float released on March 31st has a shape that changes according to the 2D flow. At the beginning of the drift at 4:00pm, it occupies an area of about 10 km along both directions whereas after 12 hours, its size is of about 30 km along latitude and 10 km along longitude [24]. The 15 m deep velocities estimated from the divergence field via the method described in Tarry *et al.* 2021 [24] reveals values ranging from

-40 m day^{-1} to 40 m day^{-1} (figure 14) on our period of time. Several hours later in the drift, velocities computed from this method can reach values of 100 m day^{-1} in absolute: these top layer high velocities can be explained by the smaller — yet comparable — scales resolved by this method (sub-mesoscale to kilometric scale). This scale difference is very important to remember further in the analysis.

In addition, the patterns described overcome the computation zone which makes their sizes impossible to identify clearly. Nevertheless, we can safely say that the plots let appear patterns of different signs that are longer than 10 km , compatible with the previous results.

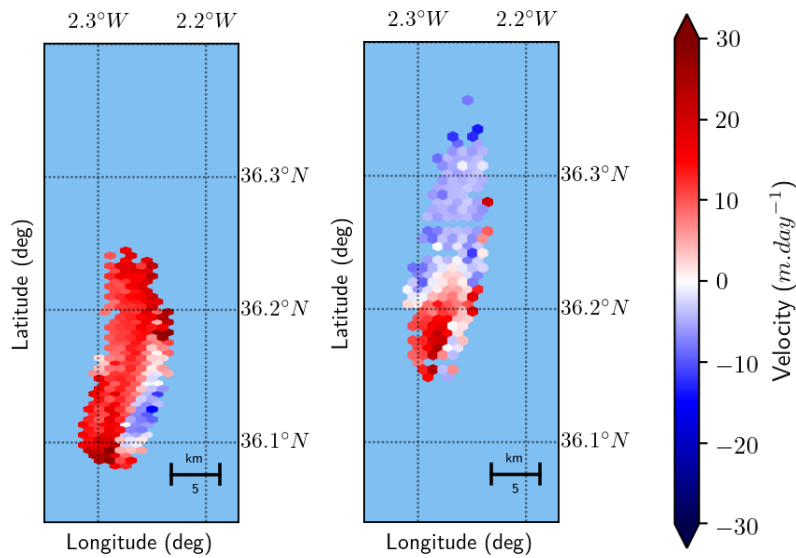


Figure 14: Vertical velocities from drifters on 1st June, 2018 at 0:20am and 3:30am.

This method lets appear as well — contrary to the data presented above — a temporal variability: the same region can change its sign and order of magnitude in about an hour (not shown). Upwelling and downwelling areas are at the same time displaced, distorted and changing in amplitude. Nevertheless, we notice very coherent values regarding results from uCTD sections. The agreement between these two methods, which are totally independent in their processing, one being Lagrangian (uCTD sections) and the other being Eulerian (surface drifters), greatly increases our level of confidence in both of their results.

4.4 Cross-checking with the continuity equation

In order to gain confidence on the vertical velocities resulting from the computations of section 3.3, we can compare it to the output of another algorithm deriving the same variable from the same data.

Assuming the incompressibility of models water parcels, the simplified continuity equation together with a null boundary condition at surface allows the integration of horizontal divergence resulting in a vertical velocities estimation (cf.: section 3.2.2). The validity of this approximation in our case is in some way compromised knowing that the IBI model considers more realistic physical processes [14] but in any case, this equation can be an interesting way of estimating the main patterns in an area or to have a look at the order of magnitude of the velocities.

Here, we compute the vertical velocities from the continuity equation using first order finite differences on the total flow, and integrate over the model vertical irregular discretization. No other processing has been done but the smoothing of unresolvable scales with a bicubic radius-based filter set at 5 km.

On figure 15, the continuity equation applied to model data reveals an alternation of patterns compatible with all previous results. Order of magnitudes are the same as the values resulting from the quasi-geostrophic omega equation, although the continuity equation method generally outputs bigger patterns. In fact, contrast between upwellings and downwellings for this algorithm is less marked and because of this, pattern sizes globally reach higher spatial dimensions. On zones with no pronounced patterns, correlation between the two methods remains unclear, but in other cases the associated *r-value*¹ can exceed the non-negligible value of 0.6. Of course, this high value is due to the very clear downwelling on the Eastern side of the eddy, but it is still worth to notice as a sign of validation.

In conclusion, the continuity equation partly confirms the quasi-geostrophic omega equation results. It agrees with it in terms of maximum observed magnitude and location of pronounced patterns. For these specific places, the vertical circulation could be driven by the geostrophic currents, and other mechanisms such as inertial waves, Ekman

¹This value ranging from -1 to 1 describes the correlation between two datasets. If the two sets are highly correlated, the *r-value* will be close to 1 in absolute, and conversely values close to 0 result from uncorrelated datasets.

5 DISCUSSION

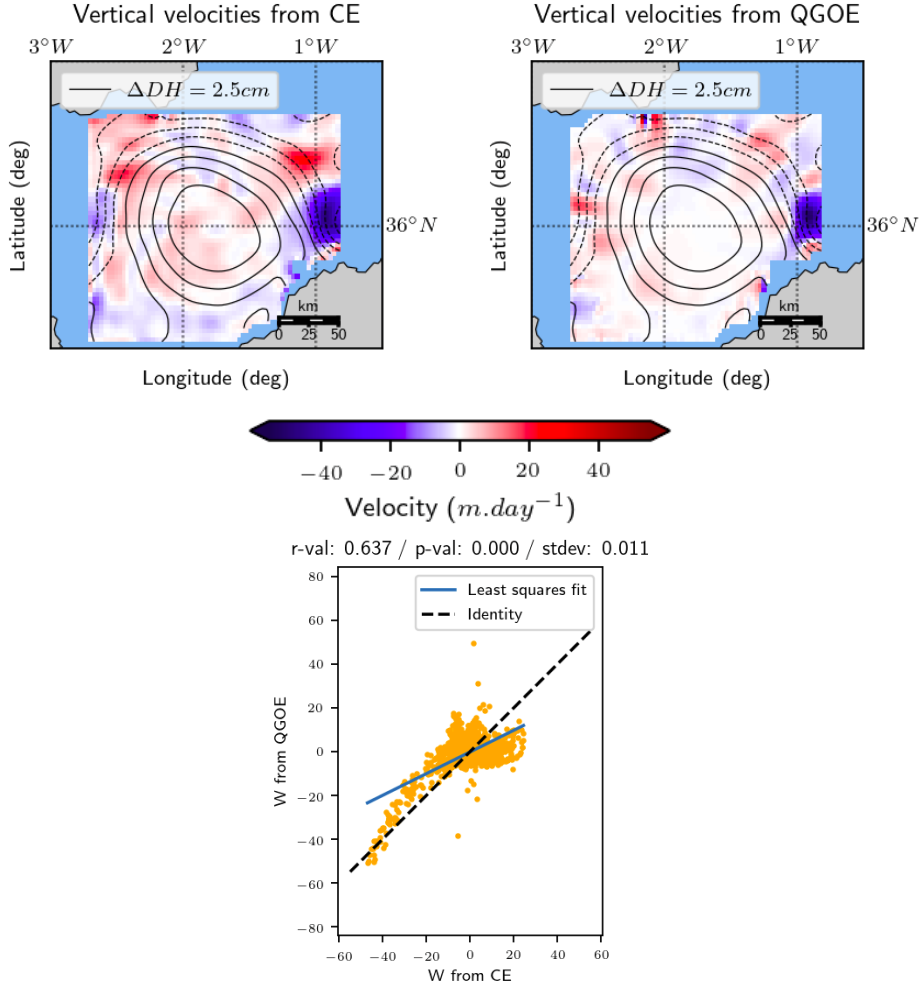


Figure 15: IBI model vertical velocities on August 14th, 2018 at 60 m from the continuity equation (top left), from the quasi-geostrophic equation (top right) and associated correlation plot (bottom).

transport...etc, only play a secondary part. The global size of the features slightly differs, as the contrast between upwellings and downwellings is higher for the quasi-geostrophic omega equation method.

5 Discussion

The fact that vertical velocities values are between three and four orders of magnitude below horizontal currents values make them very challenging to estimate or predict. In this section, we present a comparison between all previous results in order to shed light

on these difficulties.

5.1 2D flow and density structure accuracy

As the model output does not include the vertical velocity variable, we have at this point two means to check the model vertical component of the water flow: surface drifters and uCTD sections. The good agreement between these two methods allow us to bear more accurately in mind an ideal output that we would like the model to give in terms of vertical velocities. Nevertheless, it is possible to understand better the differential between the model and our reference using other variables like for example altimetry, density or also the 2D flow, which plays a serious part in the vertical velocities estimation.

Indeed, as we deduce the vertical velocity field using the horizontal currents, qualifying the quality of their representation in the model gives information about further defects. Thus, we compare the trajectory of a lagrangian particle in the model surface hourly flow to the real trajectories of nearby drifters to identify some of the model drawbacks. First, we notice a very high sensitivity of trajectories to the features location due to the strong activity of the area: on figure 16, the South-Western particle takes a completely different path than the other 8 particles, while it is just 10 km away from them. This high sensitivity relates of the crucial importance of an accurate features localization in our frame of study. Secondly, the simulated trajectories and especially the middle one have a 45° angle difference in their direction regarding the real drifter trajectory. In other words, at this date the model describes an eddy which is either distorted or tilted to the

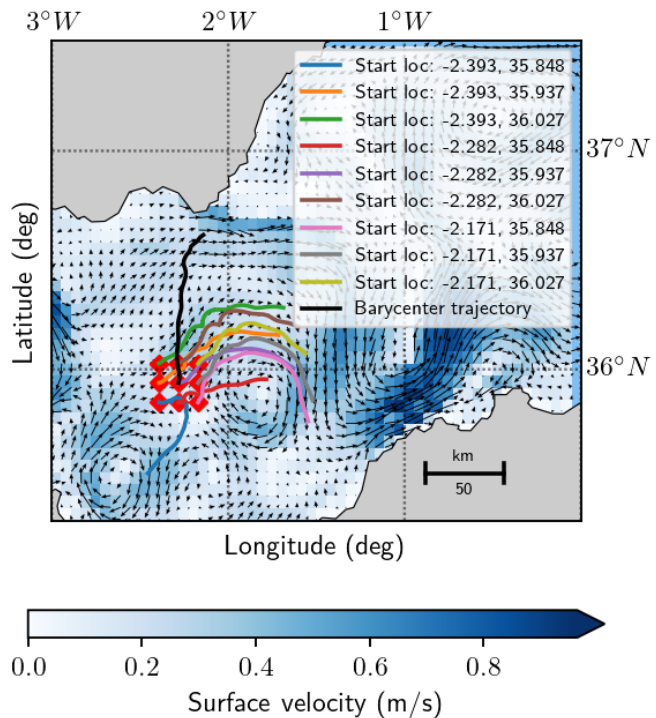


Figure 16: Barycentre 4 days trajectory of drifters number 16, 17 and 18 (black) and numerically simulated 4 days trajectories of lagrangian particles 10km spaced at $t = 0$.

right. About the intensity of the velocity field though, it fits well the drifter trajectory as all particles travel about a hundred kilometres in 3 days.

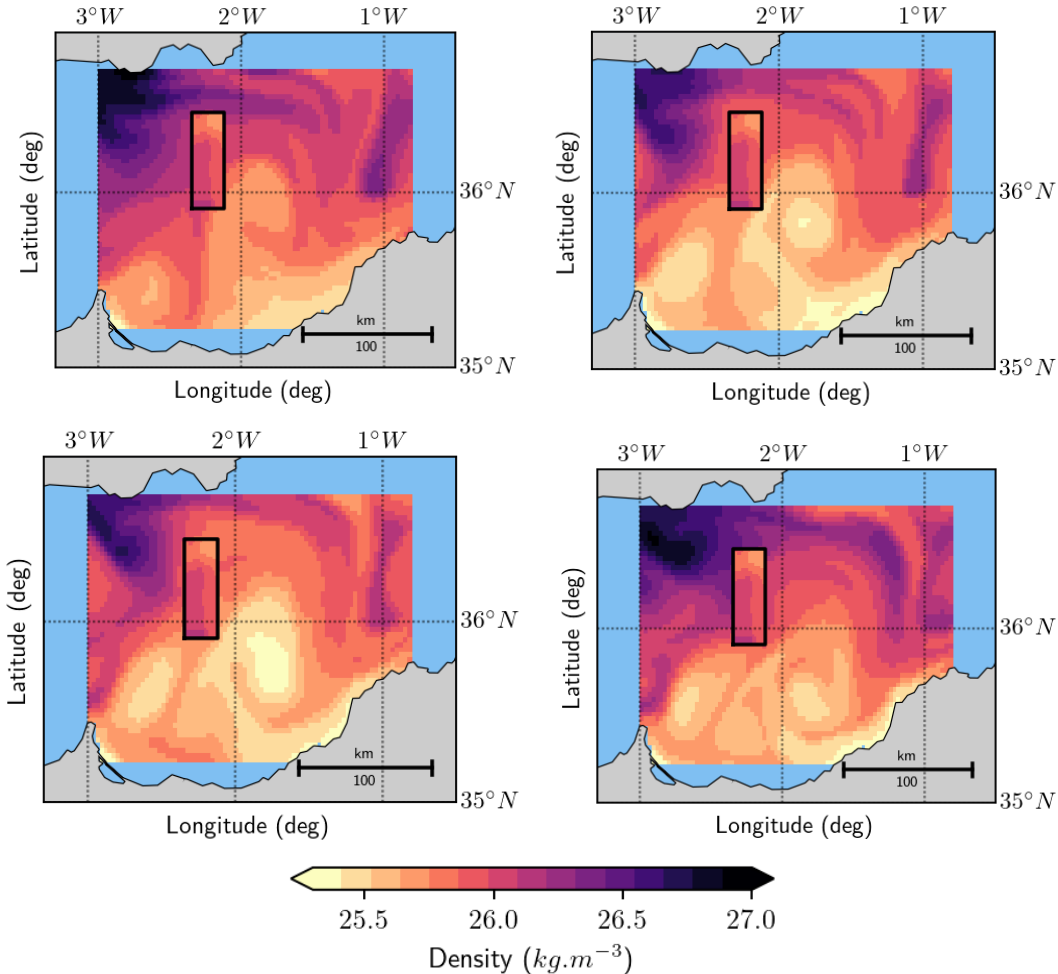


Figure 17: Model surface potential density and interpolated in-situ potential density (inside black rectangle) from May 31st to June 3rd (from left to right and top to bottom).

Furthermore, figure 17 pictures that the best fit for the uCTD sections in model data may not be the 1st but the 2nd of June regarding the density variable given by the uCTD interpolated data. At this date, the density values are very close and the front is just tilted of about 30° anticlockwise. This confirms the previous comment and at the same time adds the idea that eventually the field is being delayed of about one day. This can be explained partly by the fact that contrary to the uCTD data, the model output is daily averaged but nonetheless, the mesoscale component of the variables should not change that much significantly in less than a day. There is therefore a part played by the model

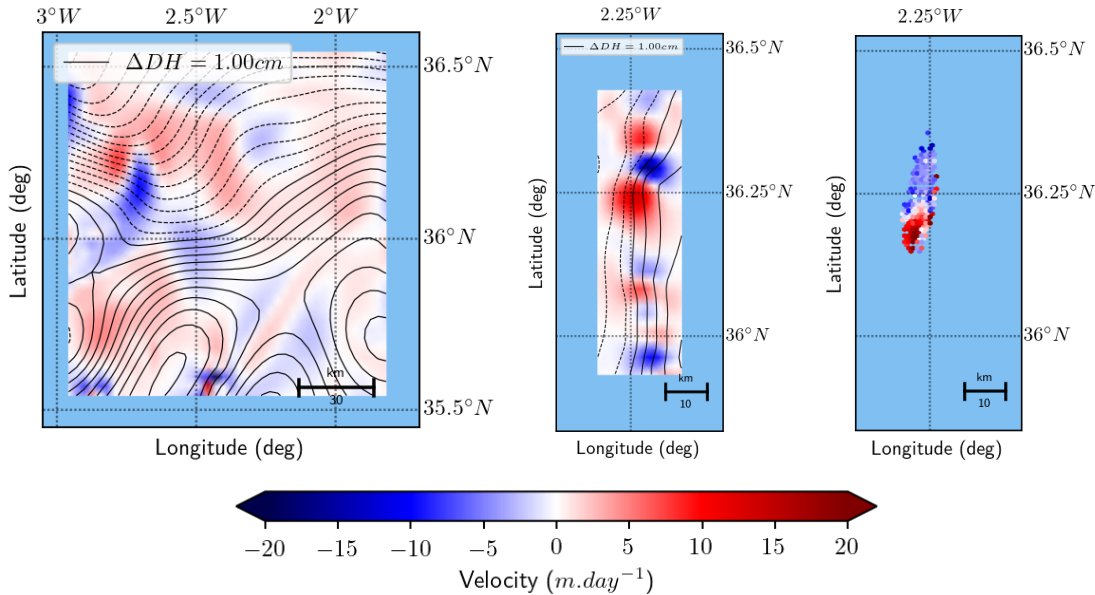


Figure 18: 10m deep vertical velocities from model on June 2nd, 2018 (left), from uCTD sections on June 1st at 10m (middle) and from drifter float on June 1st at 3:30am at 15m (right).

which will result in displacement of vertical velocities as well in the next section. An increased weight granted to the assimilation of satellite altimetry in the model code may enhance the representation of major features, as the altimetry record printed on top of figure 10 suggested correctly a meridionally aligned front.

5.2 Vertical velocities representation

When it comes to quantifying the performances of the IBI model regarding vertical velocities, we have to define what would be an ideal output associated to our reference field measurements. On June 1st, 2018, the date of the Calypso 2018 experiment, we would expect maximum velocities up to a hundred meters per day in absolute, looking at the uCTD sections results. At 10m, maximum velocities should reach about $20\ m\ day^{-1}$ taking into consideration both surface drifter and uCTD estimations. As the model variables are more alike the field measurements on June 2nd than on June 1st, we rather analyse the output of this day in order to compensate for the previously mentioned delay of the model, and use a configuration of model variables closer to measurements.

On figure 18, the model velocities at 10m reach about $10\ m\ day^{-1}$ North-West of the real front location where the dynamic height lines are the narrowest. At the real

front location, the area is less active and barely even draws the usual upwellings and downwellings. Even if it remains unclear, the front represented by the model corresponding to the sampled location may be the one occurring at $2.5^{\circ}W$, $35.9^{\circ}N$, and this feature lets appear velocities of about 5 m day^{-1} . The strongest model velocities along this particular geostrophic current are found at a depth of 90m, and range from -20 m day^{-1} to 20 m day^{-1} . Previous studies are in agreement with these extreme values in the Alboran sea [31, 34, 35]. Nevertheless in the case of uCTD data, both on surface and at 90 m, results reach 4 times these values. This underestimation of the velocities seems to reside partly in the difference in terms of dynamic height smoothness: as the intensity of the velocities is partly due to the dynamic height turns, the sharp turns of the uCTD dynamic height lines creates more intense velocities. As both model and uCTD results have been smoothed by the same bicubic filter, the difference resides in fact in the inputs very essences. In the case of surface drifters which outputs similar values in the top layer, an underestimation can be expected due to the smaller resolved scales of the method. Deeper investigation related to the influence of resolved scales would be useful to understand more clearly the extent of this issue.

Let us consider now the upwelling and downwelling patterns. According to the uCTD data, patterns should be aligned along the jet and reach an horizontal size of the order of magnitude of 10 km . In our case, the patterns are aligned correctly along the jet that nonetheless roughly makes a right angle with the reference uCTD front. In addition, the size of the patterns at surface reach about 30 km instead of 10 km . This can be attributed as well to the smoothness of the dynamic lines which have a curvature radius changing sign more often in the case of the uCTD data. As the sign of this radius is generally at the origin of a sign change in the vertical component of the flow, more smoothness draws long-lasting patterns.

On a bigger area, we can suspect that the mesoscale patterns would match better the model, as the 2D circulation at this scale is more accurately represented. Finally, in spite of the difference between chosen no motion levels, we can notice a good agreement between model and uCTD maximum velocity deepness, which can in both cases be found around 100 m in early June.

6 Conclusion

The *Iberian-Biscay-Irish Ocean Analysis and Forecasting system* model has objective assets in terms of realism of its physical variables. In this report, it has not been question at all of the handling of problematic configurations of temperature or salinity, because the implemented global dynamics are quite advanced and realistic: velocities retrieved from the model variables correspond to something that could take place in a natural environment. Furthermore, the model output describes well the mesoscale patterns of the Eastern Alboran gyre in the sense that it surrounds it by an alternation of positive and negative patterns along dynamic height isolines on the sides, and leaves the interior a more passive area in terms of vertical motion. Nevertheless, issues regarding the particular velocity structures occur later on, as it takes a lot of finesse to reveal the right values at the right time and place.

Displacement of features and smoothness of the model output leads to errors on the location, intensity and pattern sizes of the vertical velocities regarding both uCTD and surface drifters results, that are quite coherent with each other. It has been shown that the model encounters these type of issues at the particular date of the Calypso 2018 experiment, which is our only source of in-situ measurements in this work. Hence, even if a part of the error report can be attributed to the quasi-geostrophic approximation that reaches its limits in parts of the domain, the prediction of actual upwellings or downwellings remains a big issue with this kind of models. Unfortunately, increasing the complexity of equations used to retrieve vertical velocities is not an option at short-term: efforts have to be made first in terms of raw variables prediction, to depict more precise features. For instance, increasing the weight of data assimilation and/or assimilate more information in the model algorithm could be a way to improve its output.

On top of this, it is clear that the lack of in-situ measurements is problematic to identify the assets and drawbacks of our modelled vertical motions. Because of this, current representation of sub-mesoscale vertical velocities is still incomplete, and connected topics knowledge is being chained down. Phytoplankton blooming and marine photosynthesis domains for instance, which are of very serious importance regarding climate change and especially greenhouse gases recycling, would greatly benefit from an enhanced representation or prediction of vertical motions. With the funding of the Calypso 2022 experiment, we can hope for more reliable in-situ measurements in the near future, that could help modellers paint a better picture of vertical velocities in the Mediterranean and in the other oceans of the globe.

7 List of Figures

1	World map of the Rossby radius (km) [10].	3
2	The Alboran sea surface circulation.	4
3	IBI model temperature and salinity profiles on June 1 st , 2018.	4
4	Satellite image of chlorophyll in the Alboran sea on January 17 th , 2018 (NASA).	5
5	Salinity and potential temperature on April 7 th , 2018 at 60 m depth from the IBI model, and resulting density using the thermodynamic equation of sea water.	6
6	From left to right and from top to bottom: the Alliance ship [15], CARTHE drifters [17, 16] (picture: S. Ruiz (IMEDEA-CSIC)), the Lagrangian float drifter equipped with ADCP (picture: S. Ruiz (IMEDEA-CSIC)), a SVP drifter [20], a CODE drifter [19] and an uCTD probe [22].	7
7	Calypso 2018 dataset: salinity vertical section from uCTD crossing the front both ways.	8
8	Model potential temperature on June 1 st , 2018 without and with 7 km radius bicubic smoothing and resulting difference.	10
9	IBI model surface values with transect location and vertical section of potential density referenced to surface level on June 1 st , 2018.	12
10	Sea Surface Height from satellite altimetry on June 1 st , 2018 (top), surface CTD transects values and kriging interpolation (bottom left), surface CTD transects location and kriging variance (bottom right).	14
11	Rossby number associated to model currents on April 7th, 2018 at surface (left) and at 150 m (right). Characteristic scale of 30 km.	16
12	Vertical velocities from IBI model variables on April 7 th , 2018 at 20 m (top left) and 60 m (top right) with section location (black line) and associated vertical section (bottom).	19
13	Vertical velocities from uCTD variables on 1 st June, 2018 at 20 m, 60 m depths with dynamic height isolines and its associated vertical section along latitude (at 2.25°N fixed longitude).	21
14	Vertical velocities from drifters on 1 st June, 2018 at 0:20am and 3:30am.	22
15	IBI model vertical velocities on August 14 th , 2018 at 60 m from the continuity equation (top left), from the quasi-geostrophic equation (top right) and associated correlation plot (bottom).	24
16	Barycentre 4 days trajectory of drifters number 16, 17 and 18 (black) and numerically simulated 4 days trajectories of lagrangian particles 10 km spaced at $t = 0$	25
17	Model surface potential density and interpolated in-situ potential density (inside black rectangle) from May 31st to June 3rd (from left to right and top to bottom).	26
18	10 m deep vertical velocities from model on June 2 nd , 2018 (left), from uCTD sections on June 1 st at 10 m (middle) and from drifter float on June 1 st at 3:30am at 15 m (right).	27

8 References

- [1] V. Masson-Delmotte, P. Zhai, A. Pirani, S. L. Connors, C. Péan, S. Berger, N. Caud, Y. Chen, L. Goldfarb, M. I. Gomis, M. Huang, K. Leitzell, E. Lonnoy, J.B.R. Matthews, T. K. Maycock, T. Waterfield, O. Yelekçi, R. Yu and B. Zhou (eds.). *IPCC, 2021: Summary for Policymakers. In: Climate Change 2021: The Physical Science Basis.* 2021.
- [2] V. M. Kattsov, E. Källén, H. Cattle, J. Christensen, H. Drange, I. Hanssen-Bauer, T. Jóhannesen, I. Karol, J. Räisänen, G. Svensson & S. Vavulin. *Future climate change: modelling and scenarios for the Arctic.* Arctic Climate Impact Assessment. 2005.
- [3] E. Mason, S. Ruiz, R. Bourdalle-Badie, G. Reffray, M. García-Sotillo & A. Pascual. *New insight into 3-D mesoscale eddy properties from CMEMS operational models in the western Mediterranean.* Ocean Sci. <https://doi.org/10.5194/os-15-1111-2019>. 2019.
- [4] C. Harris. *New Frontiers in Operational Oceanography, Chapter 16: Coupled Atmosphere-Ocean modelling.* https://www.godae.org/~godae-data/School/Chapter16_Harris_et_al.pdf. 2018.
- [5] H.-O. Pörtner, D. C. Roberts, V. Masson-Delmotte, P. Zhai, M. Tignor, E. Poloczanska, K. Mintenbeck, A. Alegría, M. Nicolai, A. Okem, J. Petzold, B. Rama, N.M. Weyer (eds.). *IPCC: Summary for Policymakers. IPCC Special Report on the Ocean and Cryosphere in a Changing Climate.* 2019.
- [6] X. Yang, L. Liu, Z. Yin, X. Wang, S. Wang & Z. Ye. *Quantifying photosynthetic performance of phytoplankton based on photosynthesis-irradiance response models.* Environmental Sciences Europe. <https://doi.org/10.1186/s12302-020-00306-9>. 2020.
- [7] D. M. Sigman & M. P. Hain. *The Biological Productivity of the Ocean.* Nature Education. 2012.
- [8] E. M. Dickman, M. J. Vanni & M. J. Horgan. *Interactive effects of light and nutrients on phytoplankton stoichiometry.* Oecologia. <https://doi.org/10.1007/s00442-006-0473-5>. 2006.
- [9] Copernicus Marine Service website, *Atlantic-Iberian Biscay Irish Ocean Physics Analysis and Forecast,* https://resources.marine.copernicus.eu/?option=com_csw&view=details&product_id=IBI_ANALYSISFORECAST_PHY_005_001. 2021.
- [10] S Ruiz, A Mahadevan, A Pascual, M. Claret, J. Tintoré & E. Mason. *New Frontiers in Operational Oceanography, Chapter 5: Multi-platform Observations and Numerical Simulations to Understand Meso and Submesoscale Processes: A Case Study of Vertical Velocities in the Western Mediterranean.* https://www.godae.org/~godae-data/School/Chapter05_Ruiz_et_al.pdf. 2018.
- [11] L. Renault, T. Oguz, A. Pascual, G. Vizoso, & J. Tintoré, *Surface circulation in the Alboran Sea inferred from remotely sensed data.* Journal of Geophysical Research. 2012.
- [12] M. A. Freilich & A. Mahadevan. *Decomposition of Vertical Velocity for Nutrient Transport in the Upper Ocean.* AMS Journals. 2019.
- [13] Copernicus Marine Service website. *About.* <https://marine.copernicus.eu/about>. 2021.
- [14] G. Madec & the NEMO team. *NEMO ocean engine.* 2016.
- [15] Centre for Maritime Research and Experimentation website. *Research, Research Vessels, NRV Alliance.* <https://www.cmre.nato.int/research/research-vessels/nrv-alliance>. 2021.

8 REFERENCES

- [16] G. Novelli, C. M. Guigand, C. Cousin, E. H. Ryan, N. J. M. Laxague, H. Dai, B. K. Haus & T. M. Özgökmen. *A Biodegradable Surface Drifter for Ocean Sampling on a Massive Scale*, Journal of Atmospheric and Oceanic Technology. 2017.
- [17] Pacific Gyre website. *Carthe Drifter*. <https://www.pacificgyre.com/carthe-drifter.aspx>. 2021.
- [18] P.-M. Poulain & R. Gerin. *Assessment of the Water-Following Capabilities of CODE Drifters Based on Direct Relative Flow Measurements*. Journal of Atmospheric and Oceanic Technology. 2019.
- [19] Scripps Institution of Oceanography website. *CODE Drifter*. <https://gdp.ucsd.edu/ldl/code/>. 2021.
- [20] Scripps Institution of Oceanography website. *Surface Velocity Program Drifter*. <https://gdp.ucsd.edu/ldl/svp/>. 2021.
- [21] E. D'Asaro. *Performance of Autonomous Lagrangian Floats*. Journal of Atmospheric and Oceanic Technology. 2003.
- [22] Teledyne Marine website. *Underway Profiling System User's Guide*. [http://www.teledynemarine.com/Documents/Brand%20Support/OCEANSCIENCE/Technical%20Resources/Manuals%20and%20Guides/Underway%20Profiling%20System%20\(UCTD\)/UCTD%20Guide_Jul18.pdf](http://www.teledynemarine.com/Documents/Brand%20Support/OCEANSCIENCE/Technical%20Resources/Manuals%20and%20Guides/Underway%20Profiling%20System%20(UCTD)/UCTD%20Guide_Jul18.pdf). 2018.
- [23] M. Dever, M. A. Freilich, B. Hodges, T. Farrar, T. Lanagan, & A. Mahadevan. *UCTD and EcoCTD Observations from the Calypso Pilot Experiment (2018): Cruise and Data Report*. Technical report. 2019.
- [24] D. R. Tarry, S. Essink, A. Pascual, S. Ruiz, P.-M. Poulain, T. Özgökmen, L. R. Centurioni, J. T. Farrar, A. Shcherbina, A. Mahadevan & E. D'Asaro. *Frontal convergence and vertical velocity measured by drifters in the Alboran Sea*. Journal of Geophysical Research. <https://doi.org/10.1029/2020JC016614>. 2021.
- [25] A. Barth, J.-M. Beckers, C. Troupin, A. Alvera-Azcárate, & L. Vandenbulcke. *divand-1.0: n-dimensional variational data analysis for ocean observations*. Geosci. <https://gmd.copernicus.org/articles/7/225/2014/>. 2014.
- [26] F. J. Millero & A. Poisson. *International one-atmosphere equation of state of seawater*. Deep Sea Research Part A, Oceanographic Research Papers. Deep Sea Research Part A. Oceanographic Research Papers. [https://doi.org/10.1016/0198-0149\(81\)90122-9](https://doi.org/10.1016/0198-0149(81)90122-9). 1981.
- [27] S. Pond & G. L. Pickard. *Introductory Dynamical Oceanography*. 1983.
- [28] J. H. Lacasce. *Geophysical Fluid Dynamics*. Section 2.4. page 50. 2015.
- [29] M. Vargas-Yáñez, F. Plaza, J. García-Lafuente, T. Sarhan, J. M. Vargas & P. Vélez-Belchi. *About the seasonal variability of the Alboran Sea circulation*. Journal of Marine Systems. [https://doi.org/10.1016/S0924-7963\(02\)00128-8](https://doi.org/10.1016/S0924-7963(02)00128-8). 2002.
- [30] J.-M. Pinot, J. Tintoré & D. Gomis. *Multivariate analysis of the surface circulation in the Balearic Sea*. Progress in Oceanography. 1995.

8 REFERENCES

- [31] D. Gomis, S. Ruiz & M. A. Pedder. *Diagnostic analysis of the 3D ageostrophic circulation from a multivariate spatial interpolation of CTD and ADCP data.* 2000.
- [32] B. J. Hoskins, I. Draghici & H. C. Davies. *A new look at the ω -equation.* Royal Meteorological Society. 1977.
- [33] A. Pascual, D. Gomis, R.L. Haney & S. Ruiz. *A Quasigeostrophic Analysis of a Meander in the Palamós Canyon: Vertical Velocity, Geopotential Tendency, and a Relocation Technique.* Journal of Physical Oceanography. [https://doi.org/10.1175/1520-0485\(2004\)034<2274:AQAOAM>2.0.CO;2](https://doi.org/10.1175/1520-0485(2004)034<2274:AQAOAM>2.0.CO;2). 2004.
- [34] J. T. Allen, D. A. Smeed, J. Tintoré & S. Ruiz. *Mesoscale subduction at the Almeria–Oran front. Part 1: Ageostrophic flow.* Journal of Marine Systems. 2001.
- [35] S. Ruiz, M. Claret, A. Pascual, A. Olita, C. Troupin, A. Capet, A. Tovar-Sánchez, J. Allen, P.-M. Poulaïn, J. Tintoré & A. Mahadevan. *Effects of Oceanic Mesoscale and Submesoscale Frontal Processes on the Vertical Transport of Phytoplankton.* JGR Oceans. <https://doi.org/10.1029/2019JC015034>. 2019.

9 Appendix

9.1 Derivation of the quasi-geostrophic omega equation

Variables:

- f : Coriolis acceleration
- θ : Latitude
- p : Pressure
- ρ : Density
- g : Gravity acceleration
- \vec{u} : Fluid velocity
- $\vec{u}_g = \begin{pmatrix} u_g \\ v_g \\ 0 \end{pmatrix}$: Geostrophic velocity
- $\vec{u}_a = \begin{pmatrix} u_a \\ v_a \\ w \end{pmatrix}$: Ageostrophic velocity

Required assumptions:

- Mesoscale: $f(\theta) \approx f_0$ (1)
 - Quasi-geostrophic velocities: $\vec{u} = \vec{u}_g + \vec{u}_a = \begin{pmatrix} u_g \\ v_g \\ 0 \end{pmatrix} + \begin{pmatrix} u_a \\ v_a \\ w \end{pmatrix}$ and $\|\vec{u}_a\| \ll \|\vec{u}_g\|$ (2)
 - Boussinesq: $\begin{cases} \rho \approx \bar{\rho}(z) + \rho'(x, y, z, t) \\ p \approx \bar{p}(z) + p'(x, y, z, t) \end{cases}$ (3)
with $\forall x, y, z, t, \frac{\partial \rho'}{\partial z}(x, y, z, t) \ll \frac{\partial \bar{\rho}}{\partial z}(z)$ and $\frac{\partial p'}{\partial z}(x, y, z, t) \ll \frac{\partial \bar{p}}{\partial z}(z)$. $\bar{\rho}$ (resp. \bar{p}) represents the ρ (resp. p) component that only depends on the z variable, and ρ' (resp. p') can be defined simply as $\rho' = \rho - \bar{\rho}$ (resp. $p' = p - \bar{p}$).
 - Hydrostatic: $\frac{\partial p}{\partial z} \approx \frac{\partial \bar{p}}{\partial z} \approx -\rho_0 g$ (4)
-

Let's start with the Navier-Stokes equation with approximation (1):

$$\begin{cases} \frac{du_g}{dt} = -\frac{1}{\bar{\rho}} \frac{\partial P}{\partial x} + f_0 v_a \\ \frac{dv_g}{dt} = -\frac{1}{\bar{\rho}} \frac{\partial P}{\partial y} - f_0 u_a \end{cases}$$

As we assume (2), we have $\frac{d}{dt} \approx \frac{\partial}{\partial t} + u_g \frac{\partial}{\partial x} + v_g \frac{\partial}{\partial y} \equiv \frac{d_g}{dt}$. We can rewrite:

$$\begin{cases} u_a = -\frac{1}{f_0} \left(\frac{1}{\bar{\rho}} \frac{\partial P}{\partial y} + \frac{d_g v_g}{dt} \right) \\ v_a = \frac{1}{f_0} \left(\frac{1}{\bar{\rho}} \frac{\partial P}{\partial x} + \frac{d_g u_g}{dt} \right) \end{cases}$$

Acknowledging further that the definition of the geostrophic flow makes it non divergent, we deduce from the continuity equation:

$$\begin{aligned}
 0 &= \frac{\partial u}{\partial x} + \frac{\partial v}{\partial y} + \frac{\partial w}{\partial z} \\
 &= \underbrace{\frac{\partial u_g}{\partial x} + \frac{\partial v_g}{\partial y}}_{=0} + \frac{\partial u_a}{\partial x} + \frac{\partial v_a}{\partial y} + \frac{\partial w}{\partial z} \\
 &= \frac{\partial u_a}{\partial x} + \frac{\partial v_a}{\partial y} + \frac{\partial w}{\partial z}
 \end{aligned} \tag{6}$$

and so injecting u_a and v_a previous formulations in equation 6:

$$f_0 \frac{\partial w}{\partial z} - \frac{1}{\rho_0} \cancel{\frac{\partial^2 p}{\partial x \partial y}} - \frac{\partial}{\partial x} \frac{d_g v_g}{dt} + \frac{1}{\rho_0} \cancel{\frac{\partial^2 p}{\partial x \partial y}} + \frac{\partial}{\partial y} \frac{d_g u_g}{dt} = 0 \iff f_0 \frac{\partial w}{\partial z} - \frac{d_g}{dt} \zeta_g = 0 \tag{7}$$

noting $\zeta_g \equiv \frac{\partial u_g}{\partial y} - \frac{\partial v_g}{\partial x}$ the geostrophic vorticity of the fluid. Equation 7 is called the quasi-geostrophic vorticity equation in literature.

In addition, the conservation of density using assumption (3) is:

$$0 = \frac{d\rho}{dt} \approx \frac{d_g \rho}{dt} = \frac{\partial \rho'}{\partial t} + u_g \frac{\partial \rho'}{\partial x} + v_g \frac{\partial \rho'}{\partial y} + w \frac{\partial \bar{\rho}}{\partial z} \tag{8}$$

Introducing the Brunt-Vassala frequency $N = \sqrt{-\frac{g}{\rho} \frac{\partial \bar{\rho}}{\partial z}}$ and injecting it in equation 8 gives:

$$0 = \frac{\partial \rho'}{\partial t} + u_g \frac{\partial \rho'}{\partial t} + v_g \frac{\partial \rho'}{\partial t} + \frac{N^2 \bar{\rho} w}{g} \tag{9}$$

To eliminate the time derivatives, we apply respectively the operators $\frac{\partial}{\partial z}$ to equation 7 and $g \cdot \nabla^2$ to equation 9. Using (4):

$$\begin{cases} \nabla^2 (\cancel{\frac{\partial}{\partial t}} + \vec{u}_g \cdot \nabla_h) p' + N^2 \bar{\rho} \nabla^2 w = 0 \\ \frac{\partial}{\partial z} (\cancel{\frac{\partial}{\partial t}} + \vec{u}_g \cdot \nabla_h) \zeta_g - f_0 \frac{\partial^2 w}{\partial z^2} = 0 \end{cases} \tag{10}$$

noting $\vec{\nabla}_h$. the operator which performs the horizontal divergence derivation. Finally, combining these two last equations results in:

$$\begin{aligned}
 & N^2 \nabla^2 w + \nabla^2 (\vec{u}_g \cdot \vec{\nabla}_h \frac{p'}{\rho}) - f_0 \frac{\partial}{\partial z} (\vec{u}_g \cdot \vec{\nabla}_h) \zeta_g + f_0^2 \frac{\partial^2 w}{\partial z^2} = 0 \\
 \iff & N^2 \nabla^2 w + f_0^2 \frac{\partial^2 w}{\partial z^2} = f_0 \frac{\partial}{\partial z} (\vec{u}_g \cdot \vec{\nabla}_h) \zeta_g - \nabla^2 (\vec{u}_g \cdot \vec{\nabla}_h g \frac{\rho'}{\rho}) \equiv 2 \vec{\nabla} \cdot \vec{Q}
 \end{aligned}$$

with $Q = \frac{g}{\rho} (\frac{\partial \vec{u}_g}{\partial x} \cdot \vec{\nabla} \rho'; \frac{\partial \vec{u}_g}{\partial y} \cdot \vec{\nabla} \rho')$. The work of Hoskins *et al.* 1977 [32] details the writing of the equation right hand side under the form of the divergence of the Q vector.

9.2 Vertical velocities numerical integration pseudo-code

The algorithm used to retrieve vertical velocities from the quasi-geostrophic omega equation can be summed up as follows, with update the auxiliary function applying to current vertical velocities W both the finite differences quasi-geostrophic omega equation given in section 3.3 and the null boundary condition:

```

def QGOE_integration(Forcing, N, epsilon=0.1):

    W = zeros(shape(Forcing))      # Initializing vertical velocities
    diff = 1.                      # Initializing other useful variables
    prev_diff = 1.
    decreasing_rate = 1.

    # Starting loop

    while decreasing_rate * 1000 > epsilon / 100 * max(abs(W)):

        prev_W = W                  # previous vertical velocities

        W = update(W, Forcing, N)   # Updating velocities

        diff = max(W - prev_W)      # Computing indicators
        decreasing_rate = diff - prev_diff
        prev_diff = diff

    return W

```